ACS OMEGA

http://pubs.acs.org/journal/acsodf

Article

Natural Nanoclay-Based Silver–Phosphomolybdic Acid Composite with a Dual Antimicrobial Effect

Andrei A. Novikov,* Adeliya R. Sayfutdinova, Maksim V. Gorbachevskii, Sofya V. Filatova, Alla V. Filimonova, Ubirajara Pereira Rodrigues-Filho, Ye Fu, Wencai Wang, Hongqiang Wang, Vladimir A. Vinokurov, and Dmitry G. Shchukin

Cite This: *ACS Omega* 2022, 7, 6728–6736

Read Online

ACCESS | Metrics & More | Article Recommendations | Supporting Information

ABSTRACT: The problem of microbial growth on various surfaces has increased concern in society in the context of antibiotic misuse and the spreading of hospital infections. Thus, the development of new, antibiotic-free antibacterial strategies is required to combat bacteria resistant to usual antibiotic treatments. This work reports a new method for producing an antibiotic-free antibacterial halloysite-based nanocomposite with silver nanoparticles and phosphomolybdic acid as biocides, which can be used as components of smart antimicrobial coatings. The composite was characterized by using energy-dispersive X-ray fluorescence spectroscopy and transmission electron microscopy. The release of phosphomolybdic acid from the nanocomposite was studied by using UV–vis spectroscopy. It was shown that the antibiotic-free nanocomposite consisting of halloysite nanotubes decorated with silver nanoparticles loaded with phosphomolybdic acid and treated with calcium chloride possesses broad antibacterial properties, including the complete growth inhibition of *Staphylococcus aureus* and *Pseudomonas aeruginosa* bacteria at a 0.5 g × L^{-1} concentration and *Acinetobacter baumannii* at a 0.25 g × L^{-1} concentration.

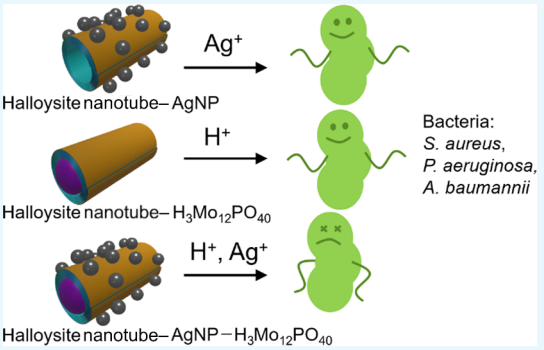

1. INTRODUCTION

The problem of microbial growth and biofilm formation on the different surfaces remains a significant concern, especially in the context of antibiotic misuse and the spreading of hospital infections.[1] Nanomaterials can serve as the antibiotic-free remedy and prevent intraclinical bacterial transmission.[2,3] Nanostructured surfaces provide mechano-bactericidal action, which could be combined with superhydrophobicity, thus preventing surface contamination.[4,5] Another promising approach is to use the biocide-release coatings that release bactericidal components that cause bacterial inactivation.[6−9] However, for most applications, the antibacterial coatings must withstand mechanical stress and combine antibacterial response and rigidity.[10,11]

Silver is a very effective practical antibacterial component. Silver nanoparticles[12] and nanorods[13] are used to combat multi-drug-resistant bacteria. Silver phosphate-based photocatalysts provide the visible-light-induced sterilization of surfaces.[14] Dual-functional surfaces based on porous amine-reactive films incorporating lubricant and silver nanoparticles (AgNPs) combined antiadhesion (passive) and bactericidal (active) properties and showed antibacterial effects toward both waterborne and airborne *Escherichia coli*.[15] Electrodeposited silver-containing calcium phosphate coatings for biomedical application produced by two methods demonstrated high antibacterial properties.[16] The antibacterial performance against *Staphylococcus aureus* was ensured by the Ag^+ ion release, whereas the secondary antibacterial effect was contact killing due to metallic AgNPs. Hydrogels based on cationic dendrimers and AgNPs demonstrated a synergetic effect in the broad spectrum of antibacterial activity against Gram-negative (*E. coli* and *Pseudomonas aeruginosa*) and Gram-positive bacteria (*Staphylococcus epidermidis* and *S. aureus*) and are promising formulations for surgical site infections.[17] The release of biocides from hydrogels is induced by acidity from growing bacteria. It was also reported that the synergetic effect on antibacterial properties is provided by combining the AgNPs and antibiotics.[18−20] The hybrid phosphotungstate ormosil materials loaded with AgNPs possessed high antibacterial performance. AgNPs were photosynthesized by UV irradiation of the phosphotungstate/SiO_2@TiO_2 heterojunction entrapped into the ormosil coating.[21] It was observed that the nanocomposite films based on cesium

Received: November 8, 2021
Accepted: January 27, 2022
Published: February 14, 2022

https://doi.org/10.1021/acsomega.1c06283
ACS Omega 2022, 7, 6728–6736

salt of phosphotungstic heteropolyacid and agarose exhibited biocidal activity promoted by the acidic surface pH.[22] Thus, heteropolyacids can be used as a biocide in antibacterial formulations. Halloysite nanotubes (HNT) are perspective nanocarriers for biocide delivery because the charged external and inner surfaces of the nanotube are suitable for modification. The biocompatibility, availability, low cost, eco-friendly profile, and hollow tubular structure make the halloysite attractive as a carrier for new antimicrobial agents.[23−26]

In this work, we report a new method for producing antibiotic-free antibacterial composites. We combined two biocides in the halloysite-based composite: AgNPs and phosphomolybdic acid (PMo). We varied preparation routes by employing different strategies to encapsulate AgNPs and PMo into the HNT. The composite demonstrated broad antibacterial properties, including the complete growth inhibition of Gram-positive (*S. aureus*) and Gram-negative (*P. aeruginosa* and *Acinetobacter baumannii*) bacteria.

2. RESULTS AND DISCUSSION

Various halloysite-based composites were produced consisting of PMo, AgNPs, or both. We assumed that the PMo encapsulation in the halloysite is affected by the solvent nature, washing procedure, and treatment with salts containing cations that reduce acid solubility. The phosphomolybdate ions tend to hydrolyze and, hence, are unstable in aqueous media.[27] It is also known that the stability of Keggin-structure phosphotungstic acid increases in organic solvents, while the proton mobility decreases.[28] Therefore, PMo was encapsulated from the ethanol solution. Composite HNT−PMo consisted of PMo encapsulated into HNT and had a bluish color that may account for the "molybdenum blue" formation due to the partial reduction of Mo^{6+} to Mo^{5+}. The composite was treated with ethanolic calcium chloride solution at pH < 1 to produce calcium salt of PMo, thus preventing the release and hydrolysis of the heteropolyanion structure during the encapsulation processes and further contact of the composite obtained with aqueous media. The HNT−PMo composites were treated by two methods. In the first method (M1), the PMo encapsulation was followed by treatment with calcium chloride. In the second method (M2), the treatment of the composite with calcium chloride was followed by PMo encapsulation. The washing procedure and encapsulation methods affect the amount of encapsulated PMo in the obtained composite, as seen by the composite color. The X-ray fluorescence (XRF) elemental analysis of HNT−PMo composites showed the differences in halloysite capacity toward PMo (Figure 1, Mo percentage indicated). Washing the wet composite with ethanol after each stage of encapsulation resulted in PMo loss from HNT. We observed the same effect after the treatment with calcium chloride ethanol solution (M1), which agrees with the visual observation of the composites (Figure 1). Although a larger amount of PMo was encapsulated in the M2 composite, we decided to compare its efficacy with that of the M1 counterpart because various processes during the encapsulation may affect the PMo release and antibacterial properties. First, acidified calcium solution may increase the protonation of outer alumina and inner silica surfaces of the halloysite, favoring the adsorption of phosphomolybdate ions. Second, calcium ions may form poorly soluble calcium phosphomolybdate, preventing the release of PMo and hydronium ions. Last but not least, the presence of calcium ions may affect the mobility of hydronium ions and their bactericidal action.

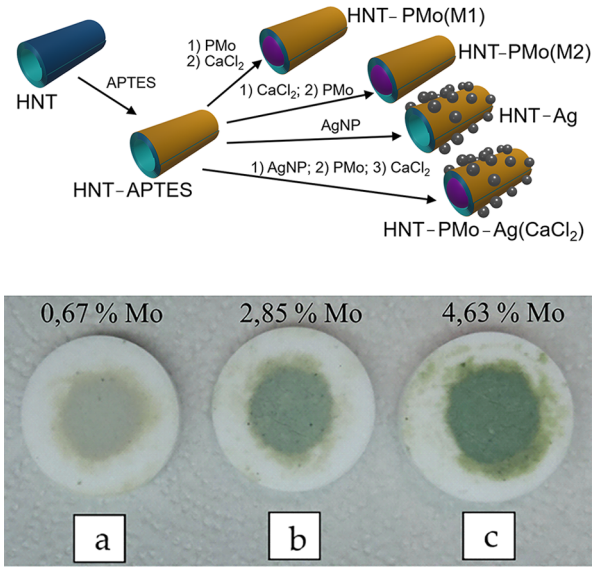

Figure 1. Overview of the obtained composites and the photograph of the HNT−PMo composites mounted on the boric acid substrates: composite washed with ethanol after encapsulation (a), composite M1 (the PMo encapsulation is followed by treatment with calcium chloride) (b), and composite M2 (the treatment of composite with calcium chloride is followed by PMo encapsulation) (c). The molybdenum content obtained by XRF analysis is indicated above the sample images. The photo was taken by one of the authors.

We performed transmission electron microscopy (TEM)−energy-dispersive X-ray spectroscopy (EDX) to characterize the distribution of phosphomolybdate in the halloysite. Phosphomolybdate ions, PMo, are composed of heavy $Mo^{6+/5+}$ ions with a larger electron cross-section than that of Al^{3+} and Si^{4+}; thus, if the acid is encapsulated inside the nanotubes, the lumen of the tube should be darker than that of the pristine halloysite (Figure 2a−c). TEM images of the HNT−PMo samples enable us to conclude that the phosphomolybdate-treated nanotubes display darker inner regions. EDX analysis of the PMo-treated nanotubes was performed to investigate this hypothesis further (Figure 2d). The presence of the Mo X-ray emission lines in the spectra (Figure 2d) of the nanotubes as well as in the X-ray mapping (Figure 2e,f), thus, establishes the darker region inside the nanotubes as being due to the encapsulated PMo.

The release of PMo from the halloysite in aqueous media was also investigated. It is expected that the release of acid from the composite will occur in contact with aqueous media and be accompanied by acidification of the media due to proton release. It was observed that the PMo−loaded halloysite (1.0 g × L^{-1}) decreases the pH of distilled water from 6 to 4, whereas the pristine halloysite dispersion (1.0 g × L^{-1}) has a pH of about 6. Therefore, it confirms that the halloysite is loaded with an acidic agent even after treatment with Ca^{2+}. Based on the spectrophotometric data, the whole amount of encapsulated PMo was released after 135 min of ultrasonication in a water medium (Figure 3). The initial stage is characterized by a burst release of 50% of the biocide within 30 min, with the time dependence being well-described by the Gompertz model.[29] The initial burst release may correspond to the rapid solubilization of PMo located between the HNT.

https://doi.org/10.1021/acsomega.1c06283
ACS Omega 2022, 7, 6728−6736

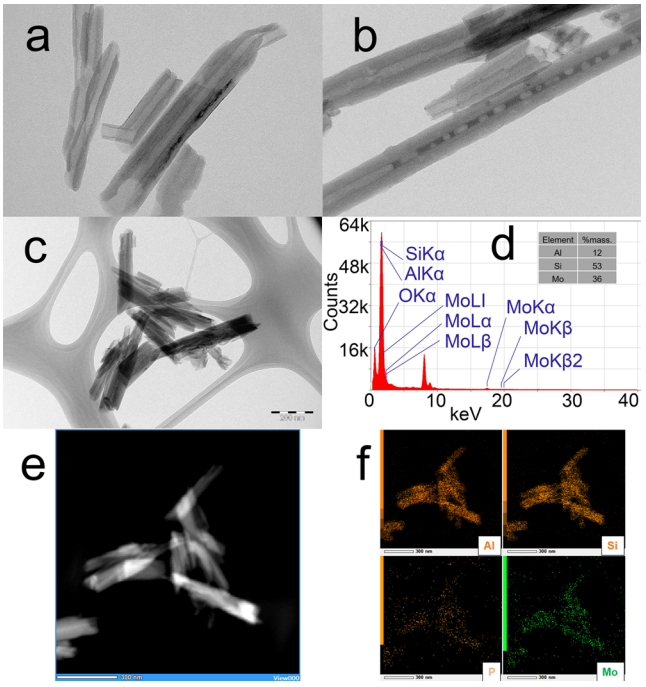

Figure 2. Study of the halloysite composite encapsulated with PMo. Brightfield TEM images of the pristine halloysite (a) and PMo-loaded halloysite (b), brightfield TEM image of the sample (c), EDX spectrum of the sample (d), STEM microphotography of the sample (e), and EDX mapping of the HNT visible in the STEM image (f).

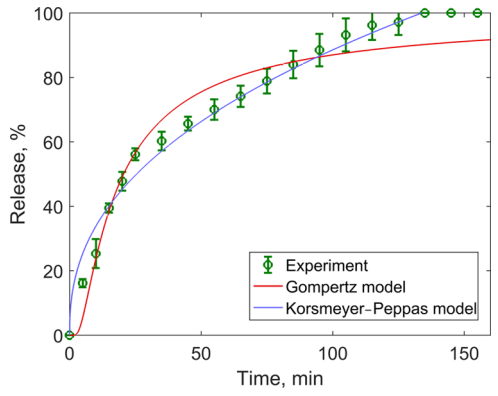

Figure 3. PMo release from the halloysite. Data points are (mean ± standard deviation) calculated from extinction at 460 nm wavelength in triplicate experiments.

However, the Gompertz model does not adequately explain the latter stages of PMo release. The Korsmeyer−Peppas model, developed for the drug release from the polymeric matrices,[30] describes the experimental data accurately at the latter stage. The model accurately predicts the complete PMo release at 135 min, and the optimized exponent parameter of 0.4174 corresponds to the low screening of the released chemical by the matrix (see also the Supporting Information).[30] The hindered diffusion of the PMo encapsulated inside the halloysite lumen could be similar to the diffusion of drugs inside a swollen polymeric matrix described by the Korsmeyer−Peppas model.

We also deposited presynthesized AgNPs onto the halloysite surface to obtain the antibacterial composite. There are many publications on this topic, including preliminary synthesis of nanoparticles followed by their deposition on the halloysite as well as in situ synthetic methods.[31−35] We have chosen to graft amino groups on the outer surface of the halloysite via silylation with (3-aminopropyl)triethoxysilane (APTES). AgNPs stabilized by sodium citrate and having a size of 20 nm were deposited onto the halloysite surface through the reaction with grafted amino groups. The morphology of HNT after immobilization of AgNPs was investigated by using TEM. We measured the AgNP size on the halloysite based on TEM image analysis. Presynthesized AgNPs did not change their initial geometric parameters during the immobilization processes onto HNT (Figure 4a,b).

We obtained HNT loaded with PMo and AgNPs (HNT−PMo−Ag) in order to evaluate the combined antibacterial effects of these agents. It is supposed that the AgNPs deposited on the surface should not agglomerate under PMo treatment since they are immobilized onto the halloysite. When exposing HNT−Ag to PMo solution in ethanol, the HNT become darker, indicating the loading with PMo, which agrees with the HNT−PMo data, with AgNPs being unchanged. It turns out that this treatment did not result in inner surface modification (Figure 4c), in opposition to the previous treatment (Figure 2b); thus, the preferable adsorption site for phosphomolybdate are the silver particles and not the surface protonated sites. Treatment of the HNT−PMo−Ag composite with the acidified solution of calcium chloride in ethanol resulted in the solution turning blue, which indicates the reduction of Mo and "molybdenum blue" formation. This process was accompanied by AgNP enlargement. The particle size and particle size distribution of immobilized AgNPs were increased as compared with that of HNT−Ag (Figure 4). EDX of the samples confirms the presence of AgNPs and compounds containing molybdenum (PMo and/or Ag_2MoO_4) (Figure 5). EDX mapping for molybdenum shows that the highest signal intensity occurs in the nanotube region, but there is a weak signal throughout the scanning area. In the case of EDX of silver, the most intense signal corresponds to electron-dense AgNPs, although there is a weak diffuse signal throughout the nanotube region, possibly indicating the partial migration of silver ions from the nanoparticles. It was observed that the replacement of Ca^{2+} with Li^+ in the treatment solution also resulted in particle agglomeration, which seems to be due to the silver−molybdenum salt formation. Interestingly, the HNT−Ag treatment according to the M2 procedure does not lead to "molybdenum blue" formation, and nanoparticle growth does not occur. This phenomenon is probably due to the formation of calcium phosphomolybdate, which prevents the redox processes involving the loaded PMo precursor.[36]

Figure 6 shows the pH dependence of the zeta potential of composites obtained. The zeta potential of halloysite-based composites is more negative than that of the pristine halloysite. The zeta potential of the HNT−PMo and HNT−PMo−Ag($CaCl_2$) suspensions decreases as the pH value increases and shows a linear downtrend. The zeta potential of HNT−PMo changes sharply due to PMo deprotonation and hydrolysis, starting from −33.6 mV and dropping to −57.4 mV, while that for HNT−PMo−Ag($CaCl_2$) changes smoothly in the investigated region of pH. The presence of AgNPs affects the zeta potential of the composite, possibly due to the interaction of silver with the encapsulated PMo.

The antibacterial properties of the obtained composite were investigated against conventional pathogens, including methicillin-sensitive *S. aureus* (MSSA), *P. aeruginosa*, and *A. baumannii*, and are presented in Figure 7. The antibacterial

https://doi.org/10.1021/acsomega.1c06283
ACS Omega 2022, 7, 6728−6736

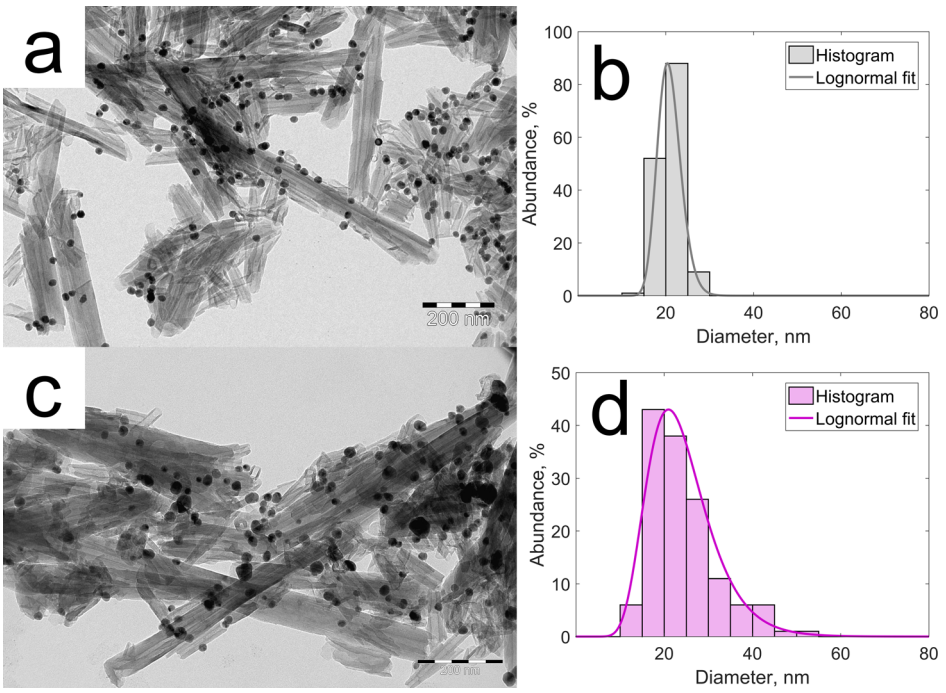

Figure 4. Brightfield TEM images (a,c) and AgNP size distributions (b,d) of samples HNT−Ag (a,b) and HNT−PMo−Ag treated with calcium chloride solution in ethanol (c,d).

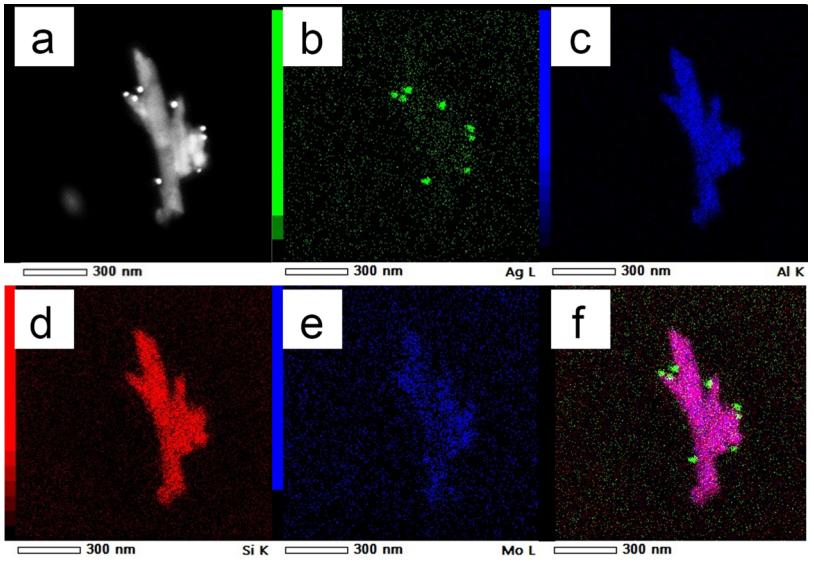

Figure 5. EDX mapping of sample HNT−PMo−Ag. STEM microphotography of sample (a), Ag mapping (b), Al mapping (c), Si mapping (d), Mo mapping (e), and overlay (f).

activity of HNT−PMo, HNT−Ag, HNT−PMo−Ag, and HNT−PMo−Ag($CaCl_2$) composites was studied. The halloysite functionalized with APTES was a control sample. We found that the HNT−PMo−Ag($CaCl_2$) composite obtained by the M2 procedure did not show significant antibacterial activity. Therefore, only the HNT−PMo−Ag($CaCl_2$) M1 composite with a silver content of 6.0 mass % by XRF data was employed for the detailed study.

We observed that the halloysite-based PMo composite does not possess antibacterial properties in the investigated range of concentrations, and the values of colony-forming units (CFUs) are at the same order of magnitude as that for the control sample. The HNT−Ag composite at high concentration reduces the growth of both Gram-positive (*S. aureus*) and Gram-negative (*P. aeruginosa* and *A. baumannii*) bacteria. Although HNT−PMo−Ag contains both tested biocides, the visible antibacterial performance was not revealed. In contrast, HNT−PMo−Ag treated with calcium chloride ethanol solution provides antibacterial activity against conventional pathogens. The minimum inhibitory concentration (MIC) values are 0.50 $g \times L^{-1}$ for *S. aureus* and *P. aeruginosa* and 0.25 $g \times L^{-1}$ for *A. baumannii*. We expected that HNT−PMo would hardly possess high antibacterial properties since the MIC of PMo is more than 1000 $\mu g \times mL^{-1}$ (for comparison, good antimicrobial agents have MIC values ranging from 0.001 to 10 $\mu g \times mL^{-1}$). It was found that the MIC values of

https://doi.org/10.1021/acsomega.1c06283
ACS Omega 2022, 7, 6728−6736

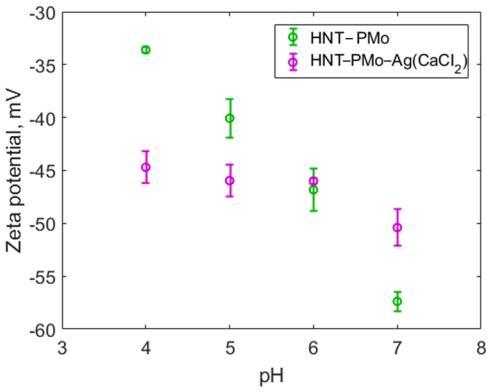

Figure 6. Zeta potential of composites vs pH.

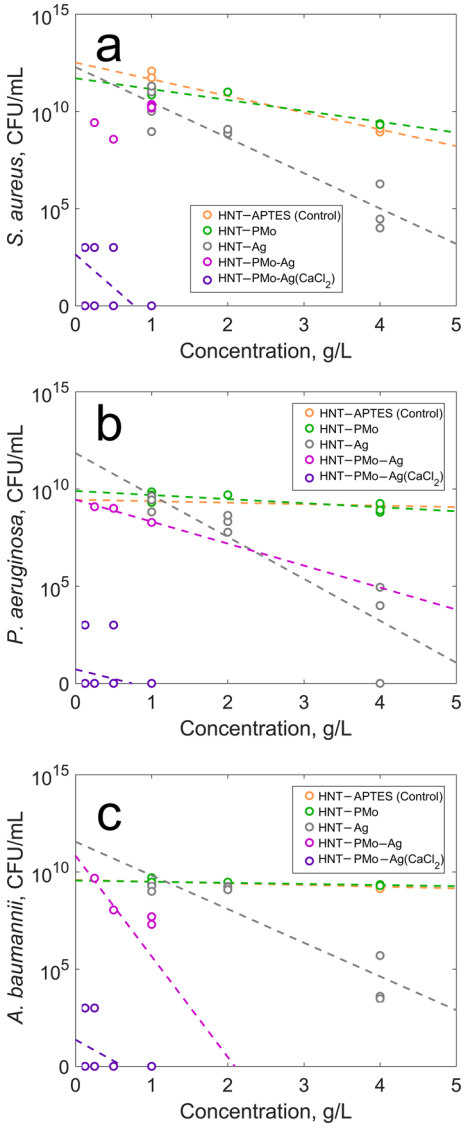

Figure 7. Antibacterial activity of composites against *S. aureus* (a), *P. aeruginosa* (b), and *A. baumannii* (c). The control sample is HNT−APTES without AgNP and PMo added. Dashed lines are linear approximations but should be treated only as a guide to the eye.

$Na_3[PMo_{12}O_{40}]\cdot nH_2O$ and $H_3[PMo_{12}O_{40}]\cdot nH_2O$ toward *S. aureus* (Gram-positive) and *E. coli* (Gram-negative) are 25.60 and 3.92 g × L^{-1}, respectively.[37,38] Some studies show that the composites based on AgNPs and halloysite exhibit antibacterial properties, but they report only growth inhibition at a certain concentration, with no MIC identified. For example, the reduction of *E. coli*[39] and *Staphylococcus marcescens* growth by the AgNP-loaded halloysite at 1 g × L^{-1} was observed.[33,40] We hypothesized that combining the halloysite and PMo with another effective biocide, such as AgNPs, would produce a composite with improved properties. We aimed to determine the MIC rather than to capture the antibacterial effect of the halloysite-based composite with PMo and AgNPs. The antibacterial performance of AgNPs strongly depends on the size, shape, and physicochemical properties of nanoparticles. The MIC of AgNPs can vary from a few micrograms per liter to hundreds and thousands of micrograms per liter. The main advantages of AgNPs having a size up to 10 nm include inducing bacterial membrane damage and penetrating the bacterial cell. It is known that the AgNPs could be oxidized to release Ag^+, with both nanoparticles and ions leading to disastrous effects on bacteria.[41] AgNPs in the HNT−Ag composite should only be considered as Ag^+ ions sources because immobilized nanoparticles cannot accumulate onto the bacterial surface as well as penetrate microbial cells and should provide ion release at the level of free nanoparticles of similar size. In this study, a high HNT−Ag concentration of 4.0 g × L^{-1} inhibits bacterial growth up to 5 orders of magnitude depending on the strain. The Ag^+ ions release from the HNT−Ag composite seems to slow down in the presence of APTES since the microbial development was slightly affected by HNT−Ag. The release rate is known to depend on the particle environment and can slow down in the presence of amino compounds, sulfides, or thiols.[42] Interestingly, the HNT−Ag composite with a high silver content (46.9%) prepared without APTES has rather low MIC values of 25 and 50 ppm against *E. coli* and *S. aureus*, respectively.[43] The untreated HNT−PMo−Ag composite does not substantially affect bacteria in this study, while the composite treated with calcium chloride exhibits antibacterial properties. We assume that this is related to the enhanced encapsulation of PMo and, possibly, to the altered silver ion migration in the presence of calcium ions. Even at concentrations of 0.25 g × L^{-1}, the composite inhibits *S. aureus* and *P. aeruginosa* growth, with complete inhibition occurring at 0.50 g × L^{-1}. The comparably high resistance of Gram-positive *S. aureus* bacteria to AgNPs was shown elsewhere.[44,45] In this study, the MIC for Gram-negative *A. baumannii* is 0.25 g × L^{-1}, that is, twice as low as that for *S. aureus*, with growth suppression observed even at 0.125 g × L^{-1}. To the best of our knowledge, the obtained composite is comparable with the composite based on reduced graphene oxide, Ag, and PMo (Ag/PMo/RGO) reported by Moghayedi et al.[46] (Table 1).

3. CONCLUSIONS

We obtained and characterized composites based on halloysite, including PMo, AgNPs, and their combination as biocides. The optimized encapsulation procedure of PMo into the halloysite lumen was developed to ensure antibacterial properties. The composite consisting of the HNT decorated with AgNPs, loaded with PMo and treated with calcium chloride, possessed superior antibacterial properties against *S. aureus*, *P. aeruginosa*, and *A. baumannii*. The growth inhibition of *S. aureus* and *P. aeruginosa* was observed at 0.25 g × L^{-1}, while that of *A. baumannii* was observed at 0.125 g × L^{-1}, with the MICs being at 0.5 and 0.25 g × L^{-1}, respectively. According to the MIC

https://doi.org/10.1021/acsomega.1c06283
ACS Omega 2022, 7, 6728−6736

Table 1. Antibacterial Properties of the Different Substances and Composites

antibacterial	MIC	bacteria	Inoculate concentration	reference
$Na_3[PMo_{12}O_{40}]\cdot nH_2O$	25.60 g × L^{-1}	*S. aureus*		38
$H_3[PMo_{12}O_{40}]\cdot nH_2O$	3.92 g × L^{-1}	*E. coli*		37
Ag/PMo/RGO	0.256 g × L^{-1}	*E.coli*	1.0 × 10^6 CFU × mL^{-1}	46
HNT−PMo−Ag (treated with $CaCl_2$)	0.5 g × L^{-1}	*S.aureus, P. aeruginosa*	1.5 × 10^6 CFU × mL^{-1}	this study
HNT−PMo−Ag (treated with CaCl2)	0.25 g × L^{-1}	*A. baumannii*	1.5 × 10^6 CFU ×m L^{-1}	this study

data found in the literature and presented in Table 1, the antibacterial properties of the obtained composite are superior to those of individual PMo and comparable with that of reduced graphene oxide with AgNPs and PMo. The composite produced in this study can be considered as a bactericidal component of smart-coating formulations.

Smart coatings may be developed using the obtained halloysite-based composites as a water-responsive functional additive. The coating surface could be hydrophobized, thus providing additional protection against bacterial colonization.[47,48] Under mechanical stress or wear, when the outer hydrophobic layer is damaged, the coating would eventually contact water or adsorb water from the air. Then, the coating will be acidified by the PMo release, and the silver ion emission will provide efficient antibacterial action.

4. MATERIALS AND METHODS

4.1. Materials. HNT, silver nitrate (99.8%), sodium citrate dihydrate (99%), and APTES (99%) were purchased from Sigma-Aldrich (St. Louis, MO, USA). PMo hydrate (80%) was purchased from Acros Organics (Geel, Belgium).

4.2. Methods. *4.2.1. Composite HNT−PMo (HNT with Encapsulated PMo) Preparation.* Halloysite was treated with 0.1 M ethanol−water solution for 30 min, centrifuged at 3000*g*, washed with ethanol, and dried. In the M1 procedure, halloysite was placed in 0.01 M PMo in ethanol under magnetic stirring for 2 h. The suspension was centrifuged, and then, the composite was placed in acidified 0.005 M $CaCl_2$ ethanolic solution under magnetic stirring for 1 h. In the M2 procedure, the composite treatment with calcium chloride was followed by PMo encapsulation. The composites obtained were centrifuged at 3000*g* and dried at 70 °C.

4.2.2. Synthesis of the HNT−PMo−Ag (HNT with Immobilized AgNPs and Encapsulated PMo) Composite. AgNPs were synthesized using the seed-growth method.[49] 200 mL of the aqueous solution containing sodium citrate (5 mM) and tannic acid (0.025 mM) was prepared and heated with a heating mantle in a three-neck round-bottomed flask for 15 min under vigorous stirring. A condenser was used to prevent the evaporation of the solvent. After boiling, 2 mL of $AgNO_3$ (25 mM) was injected into solution. The AgNPs obtained were centrifuged at 14000*g* to remove excess tannic acid. To deposit AgNPs onto the halloysite surface, NH_2 groups were grafted via silylation with APTES on the HNT. 1 g of HNT was dispersed in 50 mL of 96% ethanol solution and vigorously stirred. Next, a solution of 0.21 mL of APTES in 20 mL of 96% ethanol was added to the dispersion and left overnight under stirring at 60 °C. The modified sample was centrifuged and washed with 96% ethanol. The precipitate was dried for 24 h at 70 °C. 107 mg of HNT modified by APTES (HNT−APTES) was dispersed in 8 mL of distilled water under ultrasonication, then added to 200 mL of purified AgNPs under vigorous stirring for 12 h, then centrifuged at 2000*g*, and finally redispersed in ethanol. The suspension of HNT with immobilized AgNPs (HNT−Ag) in ethanol was then treated according to M1 and M2 procedures. The final obtained composite was centrifuged at 3000*g* and dried at 70 °C.

4.3. Material Characterization. *4.3.1. Energy-Dispersive X-ray Fluorescence Analysis.* The preweighed test sample was mounted on the boric acid substrate and placed in the EDX ARL QUANT X cuvette. The analysis was performed by a standardless procedure at atmospheric pressure.

4.3.2. TEM and EDX. For TEM analysis, the samples were dispersed in hexane. 5 μL of the dispersion was dropped on a formvar TEM grid (Ted Pella, Redding, CA, USA) and dried at room temperature. TEM micrographs were obtained using a JEM-2100 electron microscope (JEOL, Japan) at an accelerating voltage of 200 kV. EDX was performed with the JED-2300 (JEOL, Japan) analysis station. To estimate the size of AgNPs in halloysite-based composites, we used ImageJ program, allowing the measurement of diameter of particles based on the TEM image. At least 150 nanoparticle diameters were measured for each silver-based composite.

4.3.3. PMo Release Study. The PMo release was studied by the repeated sonication of the composite (10 mg) in 1 mL of water (Elmasonic S 40 H). After each 5 min sonication cycle, the sample was centrifuged, the supernatant was separated, and then, the molybdenum content was determined using UV−vis spectroscopy at 460 nm. The pellet was then replenished with water to 1 mL for the next sonication cycle.

4.3.4. Zeta Potential Measurements. The zeta potential of the samples was measured in the pH range from 4.0 to 7.0 using the SZ-100 system (Horiba, Japan) at the electric field strength of 39 V × m^{-1}.

4.3.5. Antimicrobial Assay. The clinical isolates of strain 119 (*S. aureus* MSSA), strain 12 (*P. aeruginosa*), and strain 19 (*A. baumannii*) were kindly provided by the Institute of Antimicrobial Chemotherapy (Smolensk, Russia). The method of antibacterial control was based on ISO 20776-1:2006.[50] Microplates with 96 wells were used for testing. The antibacterial activities of HNT modified by APTES (HNT−APTES) (control), HNT with encapsulated PMo (HNT−PMo), HNT with immobilized AgNPs (HNT−Ag), HNT with immobilized AgNPs and encapsulated PMo (HNT−PMo−Ag), and HNT with immobilized AgNPs and encapsulated PMo treated with calcium chloride [HNT−PMo−Ag($CaCl_2$)] against the abovementioned pathogens were studied. A suspension of the studied strains was prepared by the colony suspension method: three to five colonies from a nonselective nutrient agar medium incubated at 37 °C for 18 h were taken by a loop and moved to a sterile 0.9% sodium chloride solution. The suspension was adjusted to produce turbidity equivalent to 0.5 McFarland standard, corresponding to approximately 1.5 × 10^8 CFU × mL^{-1} of bacteria. Then, the obtained suspension was diluted to produce 1.5 × 10^6 CFU × mL^{-1} of bacteria. The tested composite sample (weighed portions of 0.5−8.0 mg) was suspended in 1.0 mL of Mueller−Hinton liquid culture medium (Becton Dickinson), and then, a

https://doi.org/10.1021/acsomega.1c06283
ACS Omega 2022, 7, 6728−6736

100 μL aliquot of the suspension was added to the microplate wells. The wells were inoculated with 100 μL of the bacterial suspension, and then, the content was mixed. The resulting concentration of the sample in the wells varied from 0.125 to 4 g × L^{-1}. Microplates were incubated at 37 °C for 18 h. After incubation, the material from each well was seeded on a universal solid nutrient medium for the quantitative counting of surviving cells. From each well, 100 μL of the suspension was taken and diluted 10^4 times, and then, 100 μL was taken from the last dilution and sown on a Petri dish with a universal solid nutrient medium. Petri dishes were incubated at 37 °C for 18 h. After incubation, the grown colonies were counted, and the number of CFUs was calculated.

■ ASSOCIATED CONTENT

Supporting Information

The Supporting Information is available free of charge at https://pubs.acs.org/doi/10.1021/acsomega.1c06283.

Equations and fitted parameters for the phosphomolybdic acid release study (PDF)

■ AUTHOR INFORMATION

Corresponding Author

Andrei A. Novikov − *Physical and Colloid Chemistry Department, Gubkin University, Moscow 119991, Russian Federation;* orcid.org/0000-0002-0887-6678; Phone: +74995078692; Email: novikov.a@gubkin.ru

Authors

Adeliya R. Sayfutdinova − *Physical and Colloid Chemistry Department, Gubkin University, Moscow 119991, Russian Federation*

Maksim V. Gorbachevskii − *Physical and Colloid Chemistry Department, Gubkin University, Moscow 119991, Russian Federation*

Sofya V. Filatova − *Physical and Colloid Chemistry Department, Gubkin University, Moscow 119991, Russian Federation*

Alla V. Filimonova − *Physical and Colloid Chemistry Department, Gubkin University, Moscow 119991, Russian Federation*

Ubirajara Pereira Rodrigues-Filho − *Institute of Chemistry of São Carlos, University of São Paulo, São Carlos 13560-970 São Paulo, Brazil*

Ye Fu − *School of Materials Science and Engineering, Beijing Technology and Business University, Beijing 100048, People Republic of China*

Wencai Wang − *Key Laboratory of Beijing City for Preparation and Processing of Novel Polymer Materials, Beijing University of Chemical Technology, Beijing 100029, People Republic of China*

Hongqiang Wang − *State Key Laboratory of Solidification Processing, Center for Nano Energy Materials, School of Materials Science and Engineering, Northwestern Polytechnical University, Xi'an 710072, People Republic of China*

Vladimir A. Vinokurov − *Physical and Colloid Chemistry Department, Gubkin University, Moscow 119991, Russian Federation;* orcid.org/0000-0002-0570-6577

Dmitry G. Shchukin − *Physical and Colloid Chemistry Department, Gubkin University, Moscow 119991, Russian Federation; Stephenson Institute for Renewable Energy, University of Liverpool, Chadwick Building, Liverpool L69 7ZF, United Kingdom;* orcid.org/0000-0002-2936-804X

Complete contact information is available at: https://pubs.acs.org/10.1021/acsomega.1c06283

Author Contributions

The manuscript was written through the contributions of all authors. All authors have approved the final version of the manuscript.

Funding

The synthesis, characterization, and antibacterial testing of nanomaterials at the Gubkin University were supported by the Russian Science Foundation (grant no. 19-79-30091).

Notes

The authors declare no competing financial interest.

■ ACKNOWLEDGMENTS

The authors thank Kirill A. Cherednichenko (Gubkin University) for the discussions.

■ ABBREVIATIONS

AgNPs, silver nanoparticles; HNT, halloysite nanotubes; PMo, phosphomolybdic acid; APTES, (3-aminopropyl)-triethoxysilane; HNT−PMo, halloysite nanotubes with encapsulated PMo; HNT−PMo−Ag, halloysite nanotubes with immobilized AgNPs and encapsulated PMo; HNT−APTES, HNT modified by APTES; HNT−Ag, halloysite nanotubes with immobilized AgNPs; TEM, transmission electron microscopy; EDX-RF, energy-dispersive X-ray fluorescence spectroscopy; HNT−PMo−Ag($CaCl_2$), halloysite nanotubes with immobilized AgNPs and encapsulated PMo treated with calcium chloride

■ REFERENCES

(1) Rawson, T. M.; Wilson, R. C.; O'Hare, D.; Herrero, P.; Kambugu, A.; Lamorde, M.; Ellington, M.; Georgiou, P.; Cass, A.; Hope, W. W.; Holmes, A. H. Optimizing Antimicrobial Use: Challenges, Advances and Opportunities. *Nat. Rev. Microbiol.* **2021**, *19*, 747−758.

(2) Wang, Y.; Yang, Y.; Shi, Y.; Song, H.; Yu, C. Antibiotic-Free Antibacterial Strategies Enabled by Nanomaterials: Progress and Perspectives. *Adv. Mater.* **2020**, *32*, 1904106.

(3) Gao, W.; Zhang, L. Nanomaterials Arising amid Antibiotic Resistance. *Nat. Rev. Microbiol.* **2021**, *19*, 5−6.

(4) Jenkins, J.; Mantell, J.; Neal, C.; Gholinia, A.; Verkade, P.; Nobbs, A. H.; Su, B. Antibacterial Effects of Nanopillar Surfaces Are Mediated by Cell Impedance, Penetration and Induction of Oxidative Stress. *Nat. Commun.* **2020**, *11*, 1626.

(5) Linklater, D. P.; Baulin, V. A.; Juodkazis, S.; Crawford, R. J.; Stoodley, P.; Ivanova, E. P. Mechano-Bactericidal Actions of Nanostructured Surfaces. *Nat. Rev. Microbiol.* **2021**, *19*, 8−22.

(6) Adlhart, C.; Verran, J.; Azevedo, N. F.; Olmez, H.; Keinänen-Toivola, M. M.; Gouveia, I.; Melo, L. F.; Crijns, F. Surface Modifications for Antimicrobial Effects in the Healthcare Setting: A Critical Overview. *J. Hosp. Infect.* **2018**, *99*, 239−249.

(7) Michailidis, M.; Sorzabal-Bellido, I.; Adamidou, E. A.; Diaz-Fernandez, Y. A.; Aveyard, J.; Wengier, R.; Grigoriev, D.; Raval, R.; Benayahu, Y.; D'Sa, R. A.; Shchukin, D. Modified Mesoporous Silica Nanoparticles with a Dual Synergetic Antibacterial Effect. *ACS Appl. Mater. Interfaces* **2017**, *9*, 38364−38372.

(8) Michailidis, M.; Gutner-Hoch, E.; Wengier, R.; Onderwater, R.; D'Sa, R. A.; Benayahu, Y.; Semenov, A.; Vinokurov, V.; Shchukin, D. G. Highly Effective Functionalized Coatings with Antibacterial and Antifouling Properties. *ACS Sustain. Chem. Eng.* **2020**, *8*, 8928−8937.

(9) Zhao, A.; Zhang, N.; Li, Q.; Zhou, L.; Deng, H.; Li, Z.; Wang, Y.; Lv, E.; Li, Z.; Qiao, M.; Wang, J. Incorporation of Silver-Embedded Carbon Nanotubes Coated with Tannic Acid into Polyamide Reverse Osmosis Membranes toward High Permeability, Antifouling, and Antibacterial Properties. *ACS Sustain. Chem. Eng.* **2021**, *9*, 11388−11402.
(10) Hasan, J.; Xu, Y.; Yarlagadda, T.; Schuetz, M.; Spann, K.; Yarlagadda, P. K. Antiviral and Antibacterial Nanostructured Surfaces with Excellent Mechanical Properties for Hospital Applications. *ACS Biomater. Sci. Eng.* **2020**, *6*, 3608−3618.
(11) Zhao, C.; Zhou, L.; Chiao, M.; Yang, W. Antibacterial Hydrogel Coating: Strategies in Surface Chemistry. *Adv. Colloid Interface Sci.* **2020**, *285*, 102280.
(12) Zhang, Y.; He, Y.; Shi, C.; Sun, M.; Yang, C.; Li, H.; Chen, F.; Chang, Z.; Zheng, X.; Wang, Z.; Dong, W.-f.; She, J.; Shao, D. Tannic Acid-Assisted Synthesis of Biodegradable and Antibacterial Mesoporous Organosilica Nanoparticles Decorated with Nanosilver. *ACS Sustain. Chem. Eng.* **2020**, *8*, 1695−1702.
(13) Seyedpour, S. F.; Dadashi Firouzjaei, M.; Rahimpour, A.; Zolghadr, E.; Arabi Shamsabadi, A.; Das, P.; Akbari Afkhami, F.; Sadrzadeh, M.; Tiraferri, A.; Elliott, M. Toward Sustainable Tackling of Biofouling Implications and Improved Performance of TFC FO Membranes Modified by Ag-MOF Nanorods. *ACS Appl. Mater. Interfaces* **2020**, *12*, 38285−38298.
(14) Su, W.; Liu, X.; Tan, L.; Cui, Z.; Liang, Y.; Li, Z.; Zhu, S.; Wu, S. Rapid Sterilization by Photocatalytic Ag3PO4/α-Fe2O3 Composites Using Visible Light. *ACS Sustain. Chem. Eng.* **2020**, *8*, 2577−2585.
(15) Lee, J.; Yoo, J.; Kim, J.; Jang, Y.; Shin, K.; Ha, E.; Ryu, S.; Kim, B.-G.; Wooh, S.; Char, K. Development of Multimodal Antibacterial Surfaces Using Porous Amine-Reactive Films Incorporating Lubricant and Silver Nanoparticles. *ACS Appl. Mater. Interfaces* **2019**, *11*, 6550−6560.
(16) Mokabber, T.; Cao, H. T.; Norouzi, N.; Van Rijn, P.; Pei, Y. T. Antimicrobial Electrodeposited Silver-Containing Calcium Phosphate Coatings. *ACS Appl. Mater. Interfaces* **2020**, *12*, 5531−5541.
(17) Dai, T.; Wang, C.; Wang, Y.; Xu, W.; Hu, J.; Cheng, Y. A Nanocomposite Hydrogel with Potent and Broad-Spectrum Antibacterial Activity. *ACS Appl. Mater. Interfaces* **2018**, *10*, 15163−15173.
(18) Lopez-Carrizales, M.; Velasco, K.; Castillo, C.; Flores, A.; Magaña, M.; Martinez-Castanon, G.; Martinez-Gutierrez, F. In Vitro Synergism of Silver Nanoparticles with Antibiotics as an Alternative Treatment in Multiresistant Uropathogens. *Antibiotics* **2018**, *7*, 50.
(19) Kaur, A.; Preet, S.; Kumar, V.; Kumar, R.; Kumar, R. Synergetic Effect of Vancomycin Loaded Silver Nanoparticles for Enhanced Antibacterial Activity. *Colloids Surf., B* **2019**, *176*, 62−69.
(20) Deng, H.; McShan, D.; Zhang, Y.; Sinha, S. S.; Arslan, Z.; Ray, P. C.; Yu, H. Mechanistic Study of the Synergistic Antibacterial Activity of Combined Silver Nanoparticles and Common Antibiotics. *Environ. Sci. Technol.* **2016**, *50*, 8840−8848.
(21) Gonçalves, L. P.; Miñán, A.; Benítez, G.; de Mele, M. F. L.; Vela, M. E.; Schilardi, P. L.; Ferreira-Neto, E. P.; Noveletto, J. C.; Correr, W. R.; Rodrigues-Filho, U. P. Self-Sterilizing Ormosils Surfaces Based on Photo-Synzthesized Silver Nanoparticles. *Colloids Surf., B* **2018**, *164*, 144−154.
(22) Piva, R. H.; Rocha, M. C.; Piva, D. H.; Imasato, H.; Malavazi, I.; Rodrigues-Filho, U. P. Acidic Dressing Based on Agarose/Cs2.5H0.5PW12O40 Nanocomposite for Infection Control in Wound Care. *ACS Appl. Mater. Interfaces* **2018**, *10*, 30963−30972.
(23) Abdullayev, E.; Price, R.; Shchukin, D.; Lvov, Y. Halloysite Tubes as Nanocontainers for Anticorrosion Coating with Benzotriazole. *ACS Appl. Mater. Interfaces* **2009**, *1*, 1437−1443.
(24) Abdullayev, E.; Sakakibara, K.; Okamoto, K.; Wei, W.; Ariga, K.; Lvov, Y. Natural Tubule Clay Template Synthesis of Silver Nanorods for Antibacterial Composite Coating. *ACS Appl. Mater. Interfaces* **2011**, *3*, 4040−4046.
(25) Lvov, Y.; Wang, W.; Zhang, L.; Fakhrullin, R. Halloysite Clay Nanotubes for Loading and Sustained Release of Functional Compounds. *Adv. Mater.* **2016**, *28*, 1227−1250.
(26) Fakhrullina, G.; Khakimova, E.; Akhatova, F.; Lazzara, G.; Parisi, F.; Fakhrullin, R. Selective Antimicrobial Effects of Curcumin@Halloysite Nanoformulation: A Caenorhabditis Elegans Study. *ACS Appl. Mater. Interfaces* **2019**, *11*, 23050−23064.
(27) Lewera, A.; Chojak, M.; Miecznikowski, K.; Kulesza, P. J. Identification and Electroanalytical Characterization of Redox Transitions in Solid-State Keggin Type Phosphomolybdic Acid. *Electroanalysis* **2005**, *17*, 1471−1476.
(28) Zhu, Z.; Tain, R.; Rhodes, C. A Study of the Decomposition Behaviour of 12-Tungstophosphate Heteropolyacid in Solution. *Can. J. Chem.* **2003**, *81*, 1044−1050.
(29) Gompertz, B. XXIV. On the Nature of the Function Expressive of the Law of Human Mortality, and on a New Mode of Determining the Value of Life Contingencies. *Philos. Trans. R. Soc. London* **1825**, *115*, 513−583.
(30) Korsmeyer, R. W.; Peppas, N. A. Effect of the Morphology of Hydrophilic Polymeric Matrices on the Diffusion and Release of Water Soluble Drugs. *J. Membr. Sci.* **1981**, *9*, 211−227.
(31) Gonchar, K. A.; Kondakova, A. V.; Jana, S.; Timoshenko, V. Y.; Vasiliev, A. N. Investigation of Halloysite Nanotubes with Deposited Silver Nanoparticles by Methods of Optical Spectroscopy. *Phys. Solid State* **2016**, *58*, 601−605.
(32) Kornilova, A. V.; Gorbachevskii, M. V.; Kuralbayeva, G. A.; Jana, S.; Novikov, A. A.; Eliseev, A. A.; Vasiliev, A. N.; Timoshenko, V. Y. Plasmonic Properties of Halloysite Nanotubes with Immobilized Silver Nanoparticles for Applications in Surface-Enhanced Raman Scattering. *Phys. Status Solidi A* **2019**, *216*, 1800886.
(33) Stavitskaya, A.; Shakhbazova, C.; Cherednichenko, Y.; Nigamatzyanova, L.; Fakhrullina, G.; Khaertdinov, N.; Kuralbayeva, G.; Filimonova, A.; Vinokurov, V.; Fakhrullin, R. Antibacterial Properties and in Vivo Studies of Tannic Acid-Stabilized Silver−Halloysite Nanomaterials. *Clay Miner.* **2020**, *55*, 112−119.
(34) Barot, T.; Rawtani, D.; Kulkarni, P. Physicochemical and Biological Assessment of Silver Nanoparticles Immobilized Halloysite Nanotubes-Based Resin Composite for Dental Applications. *Heliyon* **2020**, *6*, No. e03601.
(35) Ouyang, J.; Guo, B.; Fu, L.; Yang, H.; Hu, Y.; Tang, A.; Long, H.; Jin, Y.; Chen, J.; Jiang, J. Radical Guided Selective Loading of Silver Nanoparticles at Interior Lumen and out Surface of Halloysite Nanotubes. *Mater. Des.* **2016**, *110*, 169−178.
(36) Nagul, E. A.; McKelvie, I. D.; Worsfold, P.; Kolev, S. D. The Molybdenum Blue Reaction for the Determination of Orthophosphate Revisited: Opening the Black Box. *Anal. Chim. Acta* **2015**, *890*, 60−82.
(37) Moghayedi, M.; Goharshadi, E. K.; Ghazvini, K.; Ahmadzadeh, H.; Ludwig, R.; Namayandeh-Jorabchi, M. Improving Antibacterial Activity of Phosphomolybdic Acid Using Graphene. *Mater. Chem. Phys.* **2017**, *188*, 58−67.
(38) Yamase, T.; Fukuda, N.; Tajima, Y. Synergistic Effect of Polyoxotungstates in Combination with β-Lactam Antibiotics on Antibacterial Activity against Methicillin-Resistant Staphylococcus Aureus. *Biol. Pharm. Bull.* **1996**, *19*, 459−465.
(39) Jana, S.; Kondakova, A. V.; Shevchenko, S. N.; Sheval, E. V.; Gonchar, K. A.; Timoshenko, V. Y.; Vasiliev, A. N. Halloysite Nanotubes with Immobilized Silver Nanoparticles for Anti-Bacterial Application. *Colloids Surf., B* **2017**, *151*, 249−254.
(40) Cherednichenko, Y. V.; Evtugyn, V. G.; Nigamatzyanova, L. R.; Akhatova, F. S.; Rozhina, E. V.; Fakhrullin, R. F. Silver Nanoparticle Synthesis Using Ultrasound and Halloysite to Create a Nanocomposite with Antibacterial Properties. *Nanotechnol. Russ.* **2019**, *14*, 456−461.
(41) Zheng, K.; Setyawati, M. I.; Leong, D. T.; Xie, J. Antimicrobial Silver Nanomaterials. *Coord. Chem. Rev.* **2018**, *357*, 1−17.
(42) Le Ouay, B.; Stellacci, F. Antibacterial Activity of Silver Nanoparticles: A Surface Science Insight. *Nano Today* **2015**, *10*, 339−354.
(43) Matos, Y. B.; Romanus, R. S.; Torquato, M.; de Souza, E. H.; Villanova, R. L.; Soares, M.; Viana, E. R. Silver Nanoparticles

https://doi.org/10.1021/acsomega.1c06283
ACS Omega 2022, 7, 6728−6736

Nucleated in NaOH-Treated Halloysite: A Potential Antimicrobial Material. *Beilstein J. Nanotechnol.* **2021**, *12*, 798−807.
(44) Agnihotri, S.; Mukherji, S.; Mukherji, S. Size-Controlled Silver Nanoparticles Synthesized over the Range 5-100 Nm Using the Same Protocol and Their Antibacterial Efficacy. *RSC Adv.* **2014**, *4*, 3974−3983.
(45) Meikle, T. G.; Dyett, B. P.; Strachan, J. B.; White, J.; Drummond, C. J.; Conn, C. E. Preparation, Characterization, and Antimicrobial Activity of Cubosome Encapsulated Metal Nanocrystals. *ACS Appl. Mater. Interfaces* **2020**, *12*, 6944−6954.
(46) Moghayedi, M.; Goharshadi, E. K.; Ghazvini, K.; Ahmadzadeh, H.; Jorabchi, M. N. Antibacterial Activity of Ag Nanoparticles/Phosphomolybdate/Reduced Graphene Oxide Nanocomposite: Kinetics and Mechanism Insights. *Mater. Sci. Eng. B Solid-State Mater. Adv. Technol.* **2020**, *262*, 114709.
(47) Maayan, M.; Mani, K. A.; Yaakov, N.; Natan, M.; Jacobi, G.; Atkins, A.; Zelinger, E.; Fallik, E.; Banin, E.; Mechrez, G. Fluorine-Free Superhydrophobic Coating with Antibiofilm Properties Based on Pickering Emulsion Templating. *ACS Appl. Mater. Interfaces* **2021**, *13*, 37693−37703.
(48) Wang, T.; Huang, L.; Liu, Y.; Li, X.; Liu, C.; Handschuh-Wang, S.; Xu, Y.; Zhao, Y.; Tang, Y. Robust Biomimetic Hierarchical Diamond Architecture with a Self-Cleaning, Antibacterial, and Antibiofouling Surface. *ACS Appl. Mater. Interfaces* **2020**, *12*, 24432−24441.
(49) Bastús, N. G.; Merkoçi, F.; Piella, J.; Puntes, V. Synthesis of Highly Monodisperse Citrate-Stabilized Silver Nanoparticles of up to 200 nm: Kinetic Control and Catalytic Properties. *Chem. Mater.* **2014**, *26*, 2836−2846.
(50) ISO. Clinical laboratory testing and in vitro diagnostic test systems—susceptibility testing of infectious agents and evaluation of performance of antimicrobial susceptibility test devices—Part 2.

https://doi.org/10.1021/acsomega.1c06283
ACS Omega 2022, 7, 6728−6736